

O.I. Khrysto

Energy characteristics for nanosecond current interrupter of semiconductor-magnetic pulse generator's terminal stage

Introduction. A semiconductor diode based on reverse current interruption is used to increase a pulse amplitude and peak power delivered on the process load. Usually, a current interrupter is located in the last stage of semiconductor-magnetic pulse generator (SMPG) and is connected in parallel to the load. **Problem.** Most of publications on this topic mostly concern with analysis of physical processes in the diode structure itself within its oscillating circuit, which is separated from previous SMPG's pulse compression stages under condition of unidirectional energy transfer from the generator to the load. In this sense, the efficiency of conversion should be determined by the joint of electromagnetic interaction between non-linear compression stages, current interrupter and process load. **Goal.** Develop a mathematical model of nanosecond current interrupter to determine its electrical and energy characteristics as a part of high-voltage parallel circuit with magnetic pulse compression, depending on the duration and moment of current interruption, the equivalent circuit for load resistance, and to set the most optimal modes of its operation. **Methodology.** In this work, it is proposed to use a comprehensive approach aimed at the study of electromagnetic processes in the SMPG's circuits with a nanosecond current interrupter, which takes into account the topology of circuit, the design parameters of saturable reactor, the magnetization curve, the equivalent load's resistance, as well as the time parameters of power switches. **Results.** Analytical expressions describing the electrical and energy characteristics of the interrupter when it operating on the active load are obtained. A numerical simulation of interrupter in the SMPG's double-loop pumping circuit is carried out, taking into account a nonlinearity of SR's magnetization curve. Three operation modes of interrupter is described, depending on the initial moment of reverse conduction current interruption. The analysis of interrupter operation on the load with an active-capacitive component is carried out. **Practical meaning.** The results of research can be applied in development of high-voltage SMPG scheme with improved energy-dynamic parameters. References 20, figures 10.

Key words: semiconductor-magnetic pulse generator, nanosecond current interrupter, saturable reactor, magnetization curve, numerical simulation.

У даній роботі використовується комплексний підхід, спрямований на дослідження електромагнітних процесів у схемі магнітно-напівпровідникового генератора імпульсів з наносекундним переривником струму, який враховує топологію схеми, конструктивні параметри комутуючого дроселя, криву намагнічування його осердя, еквівалентний опір навантаження, а також часові параметри періодичної комутації силових ключів. Запропоновано модель наносекундного переривника струму паралельної ланки магнітного стиснення на основі експоненційного зростання його активного опору. Отримано аналітичні вирази, що описують електричні та енергетичні характеристики переривника струму при роботі на активне навантаження. Виконане числове модулювання переривника струму у двухконтурній схемі магнітного генератора імпульсів з урахуванням нелінійності кривої намагнічування комутуючих дроселів. Розглянуто три режими його роботи в залежності від моменту початку обриву струму зворотної провідності. Проведено аналіз роботи переривника струму на навантаження з активно-ємнісною складовою. Результати досліджень можуть бути застосовано при розробці високовольтних магнітно-напівпровідникових генераторів імпульсів з поліпшеними енергодинамічними параметрами. Бібл. 20, рис. 10.

Ключові слова: магнітно - напівпровідниковий генератор імпульсів, переривник струму, комутуючий дросель, крива намагнічування, числове моделювання.

Problem. In present, one of the promising areas of nanosecond pulse technology is the use of combination of an inductive storage and a semiconductor current interrupter in the terminate compression stage of semiconductor-magnetic pulse generator (SMPG) circuit, that allows to enhance a voltage amplitude and pulse power on the load. The majority of publications on this topic mostly concern with analysis of physical processes in the semiconductor diode structure, rather than the efficiency of energy conversion. For this reason, electrical and energy characteristics of the SMPG's terminal stage should be determined due to the compatible electromagnetic interaction between non-linear compression stages, current interrupter and electrical load. In addition, the unidirectional energy transfer from generator to the load is a separate case from the entire set of energy modes of SMPG oscillations.

Analysis of recent research and publications. SMPGs [1, 2] are a class of convertor technology, that were originally developed for powering microwave emitters and pumping gas lasers [3], where the sharpness of the pulse front plays a primary role. Over the last

decade, SMPG has become more and more widely used in electric discharge technologies for water purification and disinfection [4, 5], for air ionization by streamer discharge to remove toxic impurities [6, 7], as well as for agricultural processing [8] or food pasteurization [9]. A low-temperature plasma of barrier or corona discharges of specified technologies is a main tool for processing the primary medium (material) to eliminate harmful substances in it. Usually, the plasma of these discharges is maintained due to the release of energy from a capacitive storage, but the need to increase the peak power of pulse and energy conversion efficiency led to development of SMPG with inductive energy storage. This became possible thanks to the use, along with traditional magnetic compression stages, of semiconductor current interrupters, which are highly alloyed diodes with the effect of a sharp interruption of the reverse conduction current (SOS-diodes) [10, 11].

The traditional model of a semiconductor diode [12-14] considers a system of differential equations of the electron-hole plasma for a continuity of charged particles,

© O.I. Khrysto

the equation of an electrostatic field and thermal conductivity, which have nonlinear coefficients (mobility, ionization, and recombination) that, in turn, depend on intensity of electric field strength and temperature. At the same time, the differential equations of electric circuits do not take into account the nonlinearity of saturable reactor's (SR) magnetization curve and are considered with fixed parameters. A simultaneous solution of the hyperbolic equation for charged particles with the Poisson equation of the elliptic type can cause numerical instability, especially in the case of the sharp change in the potential between a neighboring mesh points, which exceeds 2 kT/q ratio. This circumstance requires the use of special calculation algorithms [15] (Gummel-Scharfetter difference scheme) aimed at smoothing the calculation grid. Another disadvantage of this model is that the forward and reverse conduction phases of the diode are considered from two independent circuits, provided that the SR's magnetization currents of compression stage are neglected.

A more simplified version is proposed in [16], where a high-voltage converter is modeled using an ideal current source, which changes its current through the inductance of a saturated SR according to an exponential dependence. As a result, an analytical expression was obtained that describes the pulse character on the active-capacitive load, which makes it possible to determine the energy and power released on the load. At the same time, the model does not allow to calculate the energy dissipated on the diode itself during the conversion. It is clear that energy losses in the nanosecond current interrupter (hereinafter NCI) will be determined both by the duration of the reverse current interruption and by the load parameters. In addition, for a more accurate calculation, the model should also take into account the inductive component of the electric discharge load, since the length of connecting wires can significantly affect the nature of nanosecond pulses formation.

Separation of previously unsolved part of tasks.

The experience of modeling various variants of SMPG and the analysis of existing ones, including the ones given above, shows that there are a number of issues that cannot be solved effectively, relying only on known knowledge in this area. First, when simulating a compression stage with NCI, one must take into account the nonlinear nature of the SR's magnetization curve. This is explained by the fact that in the reverse conduction circuit of diode, the discharge current of compression stage's capacitor has a complex character, consisting of two harmonic components. The first harmonic reflects the process of magnetization of the SR's core, and the second the process of its saturation. If there is no second harmonic in the reverse conduction current of the diode, it means that the SR is not saturated until the moment of interruption and the compression stage does not function properly. By changing the harmonic composition of the reverse current accordingly, it is possible to influence the current magnitude in which its interruption is realized. Secondly, it should be noted that the real technological load has a non-linear nature with a reactive component and an active resistance that can vary from units of mΩ to tens of kΩ.

Purpose of the article is to develop a mathematical model of nanosecond current interrupter to determine its electrical and energy characteristics as a part of high-voltage magnetic pulse compression parallel stage, depending on the duration and the moment of current interruption, the equivalent circuit for load resistance, and to set the most optimal modes of its operation.

Research methods: mathematical modeling of converter devices, numerical analysis for solving systems of nonlinear integro-differential equations, and approximate analytical expression of nonlinear characteristics of converter devices.

Main content of work. The operating principle of SOS diodes can be divided into two phases: in the first phase, when direct current flows, a charge accumulates in highly doped regions of the semiconductor structure; in the second phase, during the passage of the reverse current, a reverse voltage is applied to the diode, which ensures the removal of the accumulated charge from the highly doped regions with the subsequent formation of a volume charge region near the p-n junction, which leads to a sharp interruption of the current through the diode and an increase of field strength in it.

The interruption of inductive current occurs as a result of a sharp increase in the internal resistance of semiconductor NCI at the stage of reverse current conduction. The most physically close to describing a sharp current interruption is the NCI's model based on the time-dependent exponential resistance growth

$$R = R_0 \cdot \exp(\alpha \cdot t), \quad (1)$$

where α characterizes the growth rate of the interrupter resistance.

Suppose that the current break occurs at the moment of reaching the maximum of the reverse current through the NCI, when the maximum energy is stored in the inductance of SR. Then a replacement circuit will look like a parallel connection of the SR's inductance, the NCI's time-dependent active resistance and the load.

Circuit parameters are chosen as follows: the inductance of the magnetic energy storage device is $L_{sr} = 1 \mu\text{H}$, the initial current that breaks the NCI is $I_0 = 100 \text{ A}$, the initial resistance of the one is $R_0 = 0,1 \Omega$, the load resistance $R_L = 150 \Omega$.

Differential equations for an inductive circuit with a NCI:

$$L_{sr} \frac{di_0}{dt} + \frac{R_L \cdot R_0 e^{\alpha t}}{R_L + R_0 e^{\alpha t}} \cdot i_0 = 0 \quad (2)$$

is a first-order homogeneous differential equation whose solution is a function of the form:

$$i_0(t) = A \cdot \exp \left[- \int \frac{R_L \cdot R_0 e^{\alpha t}}{L_{sr} (R_L + R_0 e^{\alpha t})} dt \right], \quad (3)$$

where $A = \frac{I_0}{\exp \left[- \frac{R_L}{\alpha \cdot L_{sr}} \ln(R_L + R_0) \right]}$ – the constant,

which is determined under zero initial conditions.

The general solution of equation (3):

$$i_0(t) = \frac{I_0}{\exp\left[-\frac{R_L}{\alpha \cdot L_{sr}} \ln(R_L + R_0)\right]} \times \exp\left[-\frac{R_L}{\alpha \cdot L_{sr}} \ln(R_L + R_0 \cdot \exp(\alpha \cdot t))\right]. \quad (4)$$

Current through the NCI:

$$i_1(t) = \frac{i_0(t)}{\frac{R_0}{R_L} \exp(\alpha \cdot t) + 1}. \quad (5)$$

Current through the load:

$$i_2(t) = \frac{i_0(t) \cdot R_0 \exp(\alpha \cdot t)}{R_0 \cdot \exp(\alpha \cdot t) + R_L}. \quad (6)$$

The energy dissipated on the load:

$$E_{RL} = \int_0^{\infty} i_2^2(t) \cdot R_L dt. \quad (7)$$

$$E_{RL} = \int_0^{\infty} \frac{i_0^2(t) \cdot R_0^2 \exp(2\alpha \cdot t)}{(R_0 \cdot \exp(\alpha \cdot t) + R_L)^2} R_L dt =$$

$$= -\frac{0.5 \cdot A^2 \cdot L_{sr}}{(R_L + R_0 \cdot \exp(\alpha \cdot t))^{\frac{2R_L}{\alpha L_{sr}} + 1}} \times$$

$$\times \left(R_0 \exp(\alpha \cdot t) + L_{sr} \cdot \alpha \cdot \frac{R_L}{\alpha L_{sr} + 2R_L} \right) \Big|_0^{\infty}.$$

Since, $\lim_{t \rightarrow \infty} \frac{1}{(R_L + R_0 \exp(\alpha \cdot t))^{\frac{2R_L}{\alpha L_{sr}} + 1}} = 0$, then we

have:

$$E_{RL} = \frac{0.5 \cdot A^2 \cdot L_{sr}}{(R_L + R_0) \alpha L_{sr}} \left(R_0 + \frac{L_{sr} \cdot \alpha \cdot R_L}{\alpha L_{sr} + 2R_L} \right). \quad (8)$$

Energy dissipated on the converter:

$$E_d = \int_0^{\infty} i_1^2(t) \cdot R_0 \exp(\alpha \cdot t) dt. \quad (9)$$

$$E_d = \int_0^{\infty} \frac{i_0^2(t) \cdot R_0 \exp(\alpha \cdot t)}{(R_0 \cdot \exp(\alpha \cdot t) + R_L)^2} R_L^2 dt =$$

$$= -\frac{A^2 \cdot L_{sr} \cdot R_L^2}{(\alpha L_{sr} + 2R_L)(R_L + R_0 \exp(\alpha \cdot t))^{\frac{2R_L}{\alpha L_{sr}} + 1}} \Big|_0^{\infty}.$$

$$E_d = \frac{A^2 \cdot L_{sr} \cdot R_L^2}{(\alpha L_{sr} + 2R_L)(R_L + R_0) \alpha L_{sr}}. \quad (10)$$

The conversion efficiency is estimated as the ratio of the energy dissipated on the load, to the energy stored in the inductance L_{sr}

$$K_{eff} = \frac{\exp\left(\frac{2R_L}{\alpha L_{sr}} \ln(R_L + R_0)\right)}{(R_L + R_0) \alpha L_{sr}} \cdot \left(R_0 + \frac{L_{sr} \cdot \alpha \cdot R_L}{\alpha L_{sr} + 2R_L} \right). \quad (11)$$

Figures 1,a,c show characteristics of the instantaneous power dissipated on the load and the NCI depending on the rate of current interruption with constant load resistance $R_L = 150 \Omega$, and the Fig. 1,b,d show the corresponding characteristics of dissipated energy on the load and on the switch in the same dependence. The coefficient of exponential function for the corresponding graph: 1 – $10^{9.2}$, 2 – $10^{9.5}$, 3 – $10^{9.8}$. The quantitative value of these coefficients was chosen exactly such to provide mathematical calculations that would satisfy the nanosecond range of the interrupter's switching process duration. The time to reach a maximum power of each characteristics in Fig. 1,a respectively, is: 1 – 9,4 ns, 2 – 6,4 ns, 3 – 3,4 ns. At the same time, for maximum and minimum time of current interruption, the voltage amplitude on the load is 6 kV and 12,2 kV, respectively.

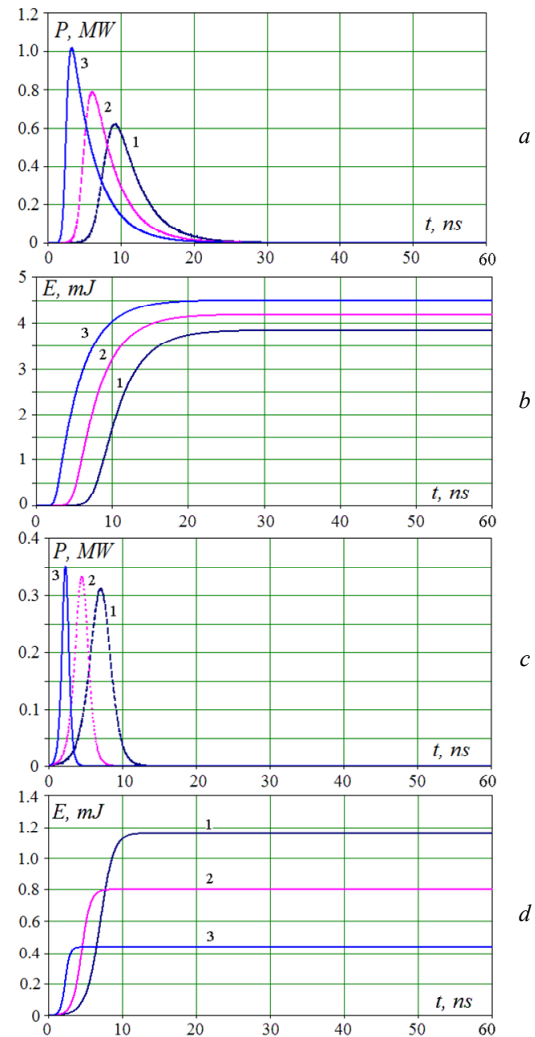


Fig. 1. Characteristics of dissipated power and energy: a) dissipated power on the load; b) dissipated energy on the load; c) dissipated power on the NCI; d) dissipated energy on the NCI

It can be seen from Fig. 1 that the peak value of the power released on the load and on the NCI are separated in time, while the characteristics have different areas, and accordingly, different dissipated energy. The energy dissipated on the load and on the NCI in the order of increasing exponential coefficient are respectively equal: $E_{RL} = 3,8 \text{ mJ}$, $4,2 \text{ mJ}$, $4,5 \text{ mJ}$; $E_d = 1,1 \text{ mJ}$, $0,8 \text{ mJ}$, $0,4 \text{ mJ}$.

Thus, as the breaking rate of current increases, the energy dissipated in the NCI decreases, and therefore the energy dissipated in the load increases.

Figure 2 shows the characteristics of energy dissipated on the load and energy dissipated on the NCI, depending on the load resistance at the fixed value of coefficient α . According to the characteristics it is clear that as the load resistance increases, the energy dissipated on the switch also increases. So for the value of the coefficient $\alpha = 10^9$, the energy dissipated on the load becomes equal to the energy dissipated on the load with the load resistance $R_L = 500 \Omega$. The real technological load, like a laser tube or a barrier discharge, is a complex parametric load, in which the discharge loop inductance and the capacitance of the electrode system are present.

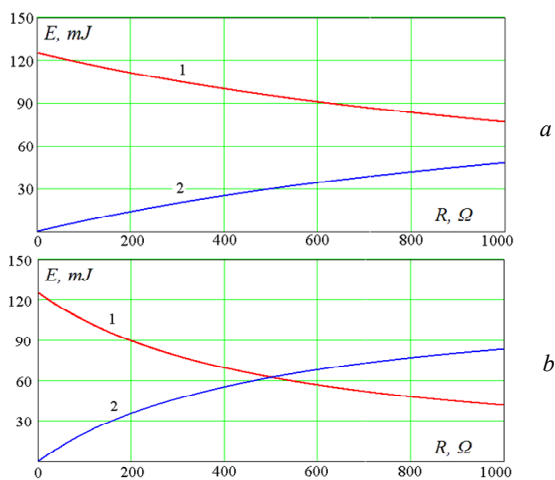


Fig. 2. Characteristic of energy dissipated on the load (1), characteristic of energy dissipated on the NCI (2), depending on the load resistance: a) $\alpha = 10^{9.5}$, b) $\alpha = 10^9$

Now consider the mutual operation of NCI with a parallel pulse compression stage. The circuit of a two-circuit pumping of a semiconductor current interrupter is shown in Fig. 3.

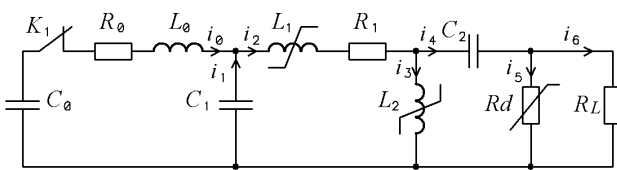


Fig. 3. The equivalent circuit for diode NCI with a terminal series-parallel compression stage

When the SR L_1 is saturated, the diode is pumped by direct current, when the SR L_2 is saturated, a reverse current of larger amplitude and shorter duration passes through the diode. Let us consider the operating regimes of the parallel compression stage when the reverse half-wave of the current is broken off with a diode at different instants of time. The SR model based on the arctangent function of the core magnetization and its provisions is described in [17]. Based on Kirchhoff's laws, a system of integro-differential equations was compiled. To determine the currents and voltages in the generator circuits, a system of algebraic equations with nonlinear coefficients was obtained using the finite-difference approximation by Euler's method [18]. Integral sums of voltages on

capacitors $C_0 - C_2$ from currents were calculated using the trapezoidal method.

Parameters of the circuit: the capacitance $C_0 = C_1 = C_2 = 2,4 \text{ nF}$, the inductance of the charging circuit is $L_0 = 120 \mu\text{H}$, the resistance of the first circuit is $R_0 = 1 \Omega$, the resistance of the second circuit is $R_1 = 0,1 \Omega$, the load resistance is $R_L = 150 \Omega$, the cores volumes of the SR's L_1 and L_2 are $V_{m1} = V_{m2} = 31,7 \cdot 10^{-6} \text{ m}^3$, the number of windings turns of the SR's L_1 and L_2 is $w_1 = 35$ and $w_2 = 10$, respectively. The step of time sampling before the current breakage was chosen equal to 2 ns, after breakage - 0.005 ns. Figure 4 shows the combined energies characteristics on the capacitors C_1 and C_2 at different moments of current interruption.

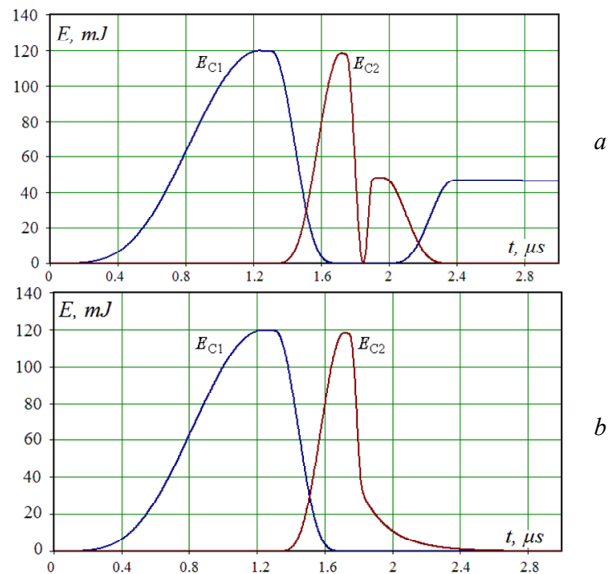


Fig. 4. Energy characteristics of pulse compression stages at different moments of the reverse current breakage through the NCI: a) when the reverse current through NCI drops; b) when the reverse current through NCI increases

Based on the simulation results, it is possible to distinguish three operation regimes of the NCI together with a series-parallel pulse compression stage. The regime when the current flowing through the inductance of the SR L_2 occurs at the half-wave current drop, is energetically inefficient, since the SR L_1 is saturated repeatedly and some of energy is returned to the capacitor of the previous compression stage (Fig. 4,a). The regime with the maximum power release occurs when the current is broken off at its maximum, when all energy is concentrated at the magnetic field of the SR L_2 inductance. The regime when the current is broken off in the first half-wave is also effective and has the advantage that it makes it possible to form a pulse on the load with a sharper leading front and a longer trailing edge. In this case, the energy is introduced into the load both from the inductive storage device L_2 and from the capacitor C_2 (Fig. 4,b). When the pulse front is formed, energy is put into the load from the inductive storage, and during the pulse trailing edge, the energy on the load is put from the capacitive storage.

The next part of the research to consider the operation of NCI diode in the composition of a parallel

stage for active-inductive and active-inductive-capacitive loads. Variants of loads are shown in Fig. 5.

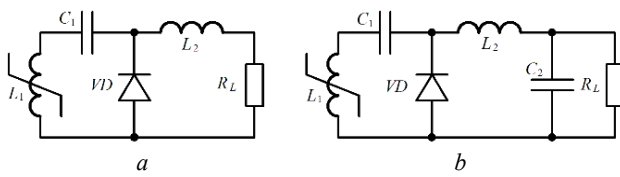


Fig. 5. The NCI load's options:
a) active-inductive; b) active-inductive-capacitive

Modeling the NCI operation on the active-inductive load. According to Fig. 6,*a,b*, when the NCI operates on the active-inductive load, the characteristic of the peak power dissipated on the load is described second-order polynomial dependence on the load resistance, and the same characteristic for the NCI has a linear increasing dependence within the active load resistance from 10 to 500 Ω . At the same time, the characteristic of energy dissipated on the load has a maximum in the range from 120 to 150 Ω , the characteristic of energy dissipated on the NCI also has an increasing linear character as the characteristic of the peak power on it.

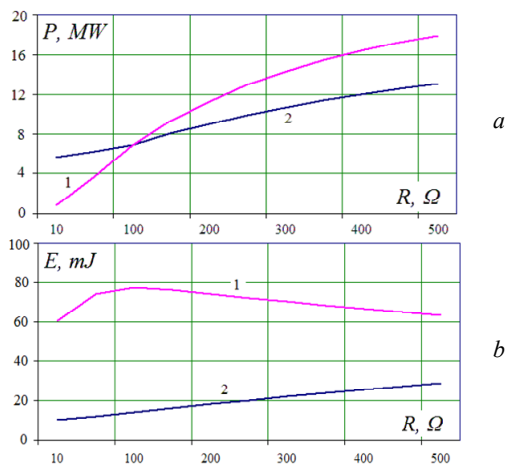


Fig. 6. Characteristics of the peak power (*a*) and energy (*b*) dissipated on the load (1) and on the NCI (2), depending on the active load resistance

Modeling the NCI operation on the active-inductive-capacitive load. Figure 7 shows the characteristics for the two load inductance values.

It is determined that if the load has a capacitive component, then maxima will appear in the characteristics of the peak power dissipated on the load. At the same time, the characteristics of the dissipated power and energy on the NCI become a linear character. It turns out that the capacitance makes it possible to stabilize the energy losses in the NCI when the active resistance of the load changes. Also, the peak power on the NCI depends on the inductive component of the load and increases with increasing it value. A sharp decrease in the characteristic in the range from 100 to 10 Ω is due to incomplete transfer of energy from the inductance of the saturated SR to the load and for a longer period of current oscillations, some of the energy from the SR inductance returns back to the longitudinal capacitor. A smooth reduction of

characteristic in the range from 200 to 500 Ω is due to a decrease in the peak current through the load.

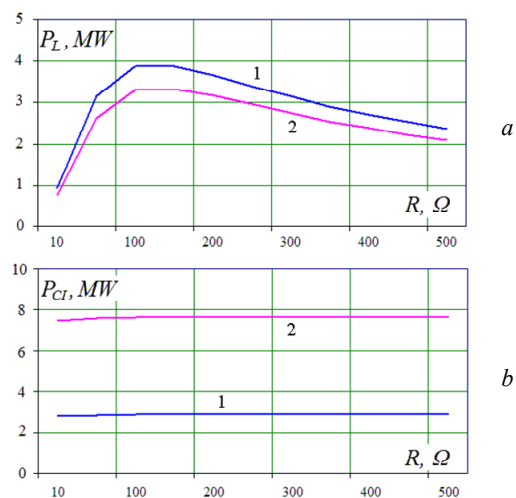


Fig. 7. Characteristics of the peak power dissipated on the load (*a*) and on the NCI (*b*) for two values of the load inductance: 1 – 100 nH; 2 – 300 nH

When the capacitance varies from 10 to 200 pF, the peak power characteristics have a decreasing nature, as shown in Fig. 8,*a*. At the same time, the characteristic falls faster on the load than on the NCI. That is, the energy losses to the NCI also stabilize when the capacitive component of the load changes. But for the characteristics of current trough the load with an increase in its capacity, there is a decrease in the sharpness of the pulse leading edge and an increase in its duration. The noted results are shown in Fig. 8,*b*.

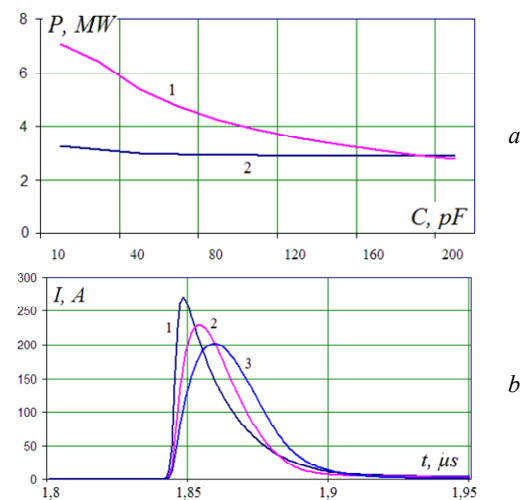


Fig. 8. Characteristics of peak power (*a*) and current characteristics in the load (*b*): a) 1 – on the load, 2 – on the NCI; b) 1 – $C = 10$ pF, 2 – 50 pF, 3 – 100 pF

Thus, the capacitive load component allows to stabilize the energy losses in the NCI current when the resistance of the active component of the load changes.

Physical modeling of a semiconductor current interrupter. To implement inductive current interruption and confirm mathematical calculations, a two-switch SMPG scheme with a parallel-serial stage in the charging circuit was used, the scheme of which is shown in Fig. 9.

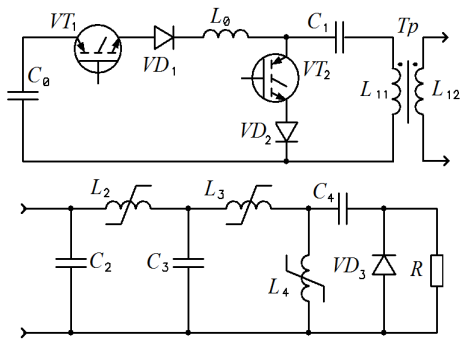


Fig. 9. A schematic diagram of two-switch SMPG with output pulse compression stage and semiconductor current interrupter

Two series-connected high-voltage diodes of the KC201E type were used as a semiconductor current interrupter. The design of these diodes is a series connection of many avalanche p-n junctions, which allows to increase the maximum allowable reverse voltage, which is proportional to the number of diodes inside the column. The maximum reverse voltage for this diode assembly is 15 kV. Electrical and structural parameters of SR $L_2 - L_4$ and capacitors $C_2 - C_4$ of the high-voltage part of the SMPG are implemented the same as in the calculation model. The load was assembled from two series power resistors, each with an active resistance of 24 Ω . A capacitive voltage divider [19] with a division ratio of 1:11000 and a low-inductive current shunt [20] with a resistance of 0,16 Ω were used to measure electrical signals on the current interrupter.

Figure 10 shows the recorded current and voltage waveforms of the semiconductor interrupter, which can be explained as follows.

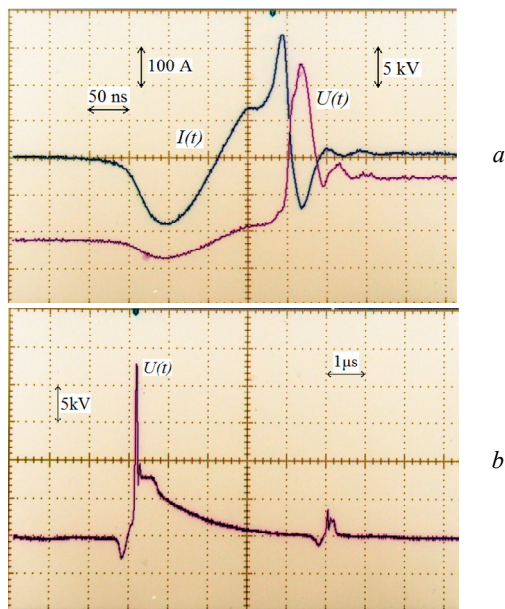


Fig. 10. Waveforms of the SMPG: a) current $I(t)$ and voltage $U(t)$ of the semiconductor interrupter VD_3 , 50 ns/div; b) voltage on the semiconductor interrupter VD_3 , 1 μ s/div

The negative half-wave of the current is caused by its flowing through the stage $VD_3 - C_3 - L_3 - C_4$ due to the turning on of the diode VD_3 in the forward direction and characterizes the process of charging the capacitor C_4 . The accumulated charge of capacitor C_4 tends to be

released through the stage $VD_3 - C_4 - L_4$, at the same time, the reverse half-wave of the current consists of two harmonic components. The first harmonic of the current has a longer period of oscillation and reflects the process of magnetization of the core of the SR L_4 , the second harmonic occurs when it is saturated and has a much shorter period of oscillation. In addition, the boundary between two states of the core has a region lasting 10 ns, for which the differential permeability of the core increases, which is reflected on the waveform as the termination of current growth. Reverse current is turned off by the diode VD_3 in approximately 25 ns. The inductive current interrupted before reaching its maximum. Therefore, the pulse on the load will have a sharp front and a long decline, which is supported by the discharge of the capacitor C_4 . At the same time, the reverse voltage developing on the diode does not exceed the allowable breakdown value for this assembly. This mode of operation of the interrupter is fully consistent with mathematical modeling and corresponds to the results indicated above.

The obtained research results were used at the Institute of Impulse Processes and Technologies of the National Academy of Sciences of Ukraine in the development of a laboratory variant of a high-voltage semiconductor-magnetic pulse generator, forming pulses with an amplitude of 30 kV, an energy of 0.2 J, a pulse repetition rate of up to 10 kHz and a duration of 80 ns, which was applied for electro-filtration of gas emissions.

Conclusions. The conducted studies show that the use of semiconductor current interrupter as part of a serial-parallel compression stage allows a radically to influence not only on the generated pulse front but also on its decline. A model of a nanosecond current interrupter based on the time-dependent exponential nature of the internal resistance growth is proposed. Analytical expressions that describe the electrical and energy characteristics of the current interrupter for a parallel circuit of its connection with an inductive storage and active load are obtained. It is shown that the dissipated energy in the load and the energy losses in the current interrupter are described by mirror functions with asymptotic behavior. Numerical modeling of a current interrupter as part of a serial-parallel circuit of magnetic pulse compression stage made it possible to distinguish three modes of its operation, the most effective of which is the current interruption mode at the maximum of stored energy in the saturable reactor inductance and the current interruption mode during its increase. In the latter case, energy is delivered in the load in two stages: during the formation of the pulse front, it is released from the inductive storage, and during the formation of the pulse decline, it is released from the capacitive one. It was found that if the load has a capacitive component, then the optimum in the peak power characteristic of the load appears in the range $R_L = 120-150 \Omega$. At the same time, the capacitive component leads to the suppression of dissipated energy on the current interrupter, so that the energy losses on it remain practically constant, independent of the load's active resistance.

Conflict of interest. The author declares no conflict of interest.

REFERENCES

1. Khrysto O. Energy transfer processes in high-voltage circuits based on magnetic pulse compression. *Acta Electrotechnica et Informatica*, 2020, vol. 20, no. 3, pp. 3-10. doi: <https://doi.org/10.15546/aei-2020-0013>.
2. Li S., Gao J., Yang H., Zhu D., Qian B., Cui Y., Wu Q., Zhang J. Investigation on Adjustable Magnetic Pulse Compressor in Power Supply System. *IEEE Transactions on Power Electronics*, 2019, vol. 34, no. 2, pp. 1540-1547. doi: <https://doi.org/10.1109/TPEL.2018.2830106>.
3. Choi J. Introduction of the magnetic pulse compressor (MPC) – fundamental review and practical application. *Journal of Electrical Engineering and Technology*, 2010, vol. 5, no. 3, pp. 484-492. doi: <https://doi.org/10.5370/JEET.2010.5.3.484>.
4. Guo X., Zheng D., Blaabjerg F. Power Electronic Pulse Generators for Water Treatment Application: A Review. *IEEE Transactions on Power Electronics*, 2020, vol. 35, no. 10, pp. 10285-10305. doi: <https://doi.org/10.1109/TPEL.2020.2976145>.
5. Boyko N.I., Makogon A.V. The micro- and nanosecond discharges in gas bubbles for water disinfection and purification. *Electrical Engineering & Electromechanics*, 2019, no. 3, pp. 50-54. doi: <https://doi.org/10.20998/2074-272X.2019.3.08>.
6. Bozhko I.V., Zozulev V.I., Kobylchak V.V. SOS-generator for the electric discharge technology used pulse barrier discharge. *Technical Electrodynamics*, 2016, no. 2, pp. 63-67. doi: <https://doi.org/10.15407/techned2016.02.063>.
7. Pokryvailo A., Yankelevich Y., Wolf M. A High-Power Pulsed Corona Source for Pollution Control Applications. *IEEE Transactions on Plasma Science*, 2004, vol. 32, no. 5, pp. 2045-2054. doi: <https://doi.org/10.1109/tps.2004.835952>.
8. Takaki K., Takahashi K., Hayashi N., Wang D., Ohshima T. Pulsed power applications for agriculture and food processing. *Reviews of Modern Plasma Physics*, 2021, vol. 5, no. 12. doi: <https://doi.org/10.1007/s41614-021-00059-9>.
9. Tamborrino A., Urbani S., Servili M., Romaniello R., Perone C., Leone A. Pulsed Electric Fields for the Treatment of Olive Pastes in the Oil Extraction Process. *Applied Sciences*, 2019, vol. 10, no. 1, art. no. 114. doi: <https://doi.org/10.3390/app10010114>.
10. Boyko N.I. Powerful generators of high-voltage pulses with nanosecond fronts. *Electrical Engineering & Electromechanics*, 2018, no. 1, pp. 59-61. doi: <https://doi.org/10.20998/2074-272X.2018.1.09>.
11. Weihua Jiang, Yatsui K., Takayama K., Akemoto M., Nakamura E., Shimizu N., Tokuchi A., Rukin S., Tarasenko V., Panchenko A. Compact solid-State switched pulsed power and its applications. *Proceedings of the IEEE*, 2004, vol. 92, no. 7, pp. 1180-1196. doi: <https://doi.org/10.1109/JPROC.2004.829003>.
12. Rukin S.N. Pulsed power technology based on semiconductor opening switches: A review. *Review of Scientific Instruments*, 2020, vol. 91, no. 1, art. no. 011501. doi: <https://doi.org/10.1063/1.5128297>.
13. Fardi H. Numerical Analysis of Semiconductor PN Junctions Using MATLABM. *Journal of Scientific Research and Reports*, 2015, vol. 6, no. 2, pp. 84-98. doi: <https://doi.org/10.9734/JSRR/2015/14434>.
14. Sharabani Y., Rosenwaks Y., Eger D. Mechanism of fast current interruption in p- π -p diodes for nanosecond opening switches in high-voltage-pulse applications. *Physical Review Applied*, 2015, vol. 4, no. 1, art. no. 014015. doi: <https://doi.org/10.1103/PhysRevApplied.4.014015>.
15. Scharfetter D.L., Gummel H.K. Large-signal analysis of a silicon Read diode oscillator. *IEEE Transactions on Electron Devices*, 1969, vol. 16, no. 1, pp. 64-77. doi: <https://doi.org/10.1109/T-ED.1969.16566>.
16. Pereverzev A.V., Litvinenko T.M. High-voltage converter for electrodischarge neutralization of sulfur dioxide. *Technical Electrodynamics*, 2015, no. 6, pp. 84-89.
17. Khrysto O.I., Zozulev V.I., Sholokh D.O. Numerical simulation of electromagnetic processes in the scheme of magnetic pulse generator. *Technical Electrodynamics*, 2014, no. 2, pp. 22-28.
18. Nurujjaman Md. Enhanced Euler's method to solve first order ordinary differential equations with better accuracy. *Journal of Engineering Mathematics and Statistics*, 2020, vol. 4, no. 1, pp. 1-13. doi: <https://doi.org/10.5281/zenodo.3731020>.
19. Anokhin Y.L., Brzhezitsky V.O., Haran Y.O., Masliuchenko I.M., Protsenko O.P., Trotsenko Y.O. Application of high voltage dividers for power quality indices measurement. *Electrical Engineering & Electromechanics*, 2017, no. 6, pp. 53-59. doi: <https://doi.org/10.20998/2074-272X.2017.6.08>.
20. Baranov M.I., Kniaziev V.V., Rudakov S.V. Coaxial disk shunt for measuring in the heavy-current chain of high-voltage generator of storm discharges of impulses of current of artificial lightning with the integral of action to $15 \cdot 10^6$ J/Ohm. *Electrical Engineering & Electromechanics*, 2017, no. 5, pp. 45-50. doi: <https://doi.org/10.20998/2074-272X.2017.5.07>.

Received 01.08.2022

Accepted 22.11.2022

Published 06.05.2023

O.I. Khrysto¹, PhD, Senior Researcher,

¹Institute of Pulse Processes and Technologies of NAS of Ukraine, 43-A, Bogoyavlenskij Avenue, Mykolayiv, 54018, Ukraine. e-mail: alexander.khristo@gmail.com

How to cite this article:

Khrysto O.I. Energy characteristics for nanosecond current interrupter of semiconductor-magnetic pulse generator's terminal stage. *Electrical Engineering & Electromechanics*, 2023, no. 3, pp. 59-65. doi: <https://doi.org/10.20998/2074-272X.2023.3.09>